Surface electronic structure of Mn/Si(111)-$\sqrt{3}\times\sqrt{3}$

J. Hirvonen Grytzelius,* H. M. Zhang, and L. S. O. Johansson
Department of Physics, Karlstad University, S-651 88 Karlstad, Sweden

(Received 26 May 2008; revised manuscript received 9 September 2008; published 6 October 2008)

The Mn/Si(111)-$\sqrt{3}\times\sqrt{3}$ surface has been studied in detail by low energy electron diffraction (LEED), angle-resolved photoelectron spectroscopy (ARPES), and core-level photoelectron spectroscopy (CLS). Annealing of the deposited manganese resulted in a well-ordered surface as seen by intense $\sqrt{3}\times\sqrt{3}$ LEED spots. ARPES spectra recorded in the $\bar{\Gamma}$-$\bar{K}$-$\bar{M}$ direction of the $\sqrt{3}\times\sqrt{3}$ surface Brillouin zone show five surface related features in the band gap while in the $\bar{\Gamma}$-$\bar{M}$-$\bar{\Gamma}$ direction four surface features are observed. The high-resolution Si 2*p* CLS data were recorded at photon energies between 108–140 eV both at normal and 60° emission angle. The bulk component was identified from the bulk sensitive spectrum recorded at a photon energy of 108 eV. To achieve a consistent core-level fitting over the whole energy and angular range, five components were introduced in the line-shape analysis. The photoemission data from the $\sqrt{3}\times\sqrt{3}$ surface have been discussed and compared with a recent theoretical model. The findings here support a layered Mn silicide film structure.

DOI: 10.1103/PhysRevB.78.155406 PACS number(s): 79.60.−i, 68.35.bg, 68.35.bj

I. INTRODUCTION

The interest in transition metals on well defined semiconductors has increased over the last years. One main reason is the possibility to combine semiconducting and magnetic properties. The ability to use the spin degree of freedom of the electron in the standard charge-based electronics could lead to a tremendous improvement in data storage and memory handling.[1] It is, however, important to understand the fundamental properties of those materials that are candidates for applications in the field of spintronics.

Not much has been reported about the complex surface grown when depositing a few monolayers (ML) of Mn on Si(111), where one monolayer is defined as the number of topmost atoms in the unreconstructed Si(111) surface. The low coverage regime has been investigated with scanning tunneling microscopy (STM) by several groups reporting surface morphology dependence on deposition rate, substrate, and temperature.[2,3] A modified Volmer-Weber growth mode with island formation for a coverage up to 4 ML has been observed.[4] The growth and structural properties have been studied for Mn silicide films up to 100 Å on Si(111)-($\sqrt{3}\times\sqrt{3}$):Bi and Si(111)-7×7.[5–8] MnSi or γ-Mn was found to directly grow on a Mn induced $\sqrt{3}\times\sqrt{3}$ reconstructed surface.[7] The formation of manganese monosilicide films by codeposition of Mn and Si has been studied using x-ray absorption, core-level, and valence-band spectroscopies.[9,10] Investigation of epitaxially grown manganese silicide by angle-integrated valence-band photoemission spectroscopy (PES) as well as Si 2*p* core-level spectroscopy has shown a strain dislocation in the film at a coverage of 5 ML.[11] A nonmetal to metal transition depending on the thickness of the film has also been reported.[12] In addition, a temperature dependence for the formation of manganese silicides with different ratios has also been studied.[13]

In this paper we present our experimental results regarding the electronic structure of Mn/Si(111)-$\sqrt{3}\times\sqrt{3}$. The surface has been investigated in detail by angle-resolved valence-band and core-level spectroscopies. The Mn/Si(111)-$\sqrt{3}\times\sqrt{3}$ surface shows two continuous bands and three partially resolved bands in the band gap. The high-resolution Si 2*p* core-level spectra recorded at different photon energies and with different emission angles show four core-level components which differ from those reported in earlier studies.[9,11]

II. EXPERIMENTAL DETAILS

The photoemission study was performed at beamline 33 at the MAX-lab synchrotron-radiation facility in Lund, Sweden.[14] The energy resolution of the angle-resolved valence-band spectra presented here is ~50 meV with an angular resolution of ±2°. The Si 2*p* core-level spectra were obtained with an energy resolution of ~90 meV and an angular resolution of ±2°. The pressure during evaporation was $\sim 1\times 10^{-10}$ mbar, which is also similar during measurements. Si(111) samples were cut from a Sb-doped (1 Ω cm) single-crystal wafer and prepared by an etching method. The Si(111) samples were cleaned *in situ* by stepwise direct current heating up to 930 °C followed by rapid flash heating up to 1230 °C. This procedure resulted in a well-ordered 7×7 surface as seen by low energy electron diffraction (LEED). Manganese was evaporated from a well outgassed electron-beam evaporator (Omicron/Focus) at a rate of 0.5 ML/min. The evaporator was carefully calibrated by a quartz-crystal monitor. Evaporation of 3 ML of manganese followed by postannealing at ~400 °C for 5 min resulted in an intense $\sqrt{3}\times\sqrt{3}$ LEED pattern as seen in Fig. 1. In our preliminary STM studies,[15] the film thickness was estimated to ~5–8 Å. Also, the topographic STM images show a very well-ordered $\sqrt{3}\times\sqrt{3}$ reconstructed surface.

The work function has been determined by measuring the total width of the valence-band spectra from the low energy cutoff to the Fermi level (E_F) at a photon energy of 21.2 eV and a sample bias of −9.56 V. The value obtained for the Mn/Si(111)-$\sqrt{3}\times\sqrt{3}$ surface is 4.57 eV. The pinning position of the Fermi level with respect to the valence-band maxi-

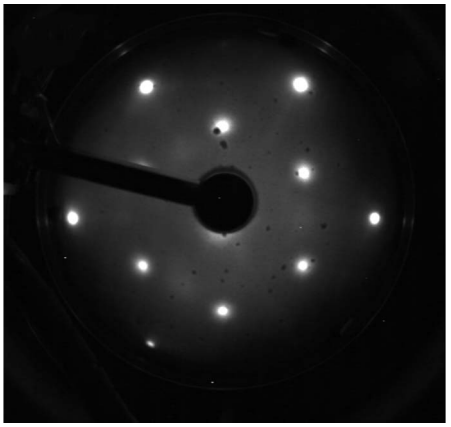

FIG. 1. LEED image of the Mn/Si(111)-$\sqrt{3}\times\sqrt{3}$ surface. The sample temperature was 100 K and the primary energy of the electrons was 46 eV. The intense $\sqrt{3}$-diffraction spots are clearly seen.

mum was estimated by comparing high-resolution Si $2p$ spectra recorded at 130 eV for the clean Si(111)-7×7 and the Mn/Si(111)-$\sqrt{3}\times\sqrt{3}$ surfaces. With a reference value of 0.65 eV for the Si(111)-7×7 surface,[16] we obtain a value of 0.60 eV for the Mn/Si(111)-$\sqrt{3}\times\sqrt{3}$ surface.

III. RESULTS AND DISCUSSION

Figure 2(a) shows a set of angle-resolved photoemission spectra from the $\sqrt{3}\times\sqrt{3}$ surface recorded at 100 K along the $\bar{\Gamma}$-$\bar{K}$-$\bar{M}$ line of the surface Brillouin zone (SBZ). The spectra show a clear metallic character as seen by the sharp Fermi edge. In the $\bar{\Gamma}$-$\bar{K}$-$\bar{M}$ direction five surface related features are observed and are labeled as S_1–S_5. Figure 2(b) shows a set of spectra recorded along the $\bar{\Gamma}$-$\bar{M}$-$\bar{\Gamma}$ line of the $\sqrt{3}\times\sqrt{3}$ SBZ. In this direction four surface features that are spectrally resolved can be correlated with four of the surface features seen in the $\bar{\Gamma}$-$\bar{K}$-$\bar{M}$ direction. These surface related features presented here may be related to both the "bulk" of the Mn silicide film and the Mn silicide surface.

In the $\bar{\Gamma}$-$\bar{K}$-$\bar{M}$ direction S_1 is well resolved between emission angles 8° and 20°, and reaches its maximum at an emission angle of 16°. In the $\bar{\Gamma}$-$\bar{M}$-$\bar{\Gamma}$ direction S_1 appears quite weak in intensity at small emission angles. With higher emission angles, it is becoming more intense and appears as a distinct peak. In the $\bar{\Gamma}$-$\bar{K}$-$\bar{M}$ direction the surface state S_2 is best resolved at small emission angle between 0° and 8°, and 36°. S_2 is weak in intensity over the whole angular range in both the $\bar{\Gamma}$-$\bar{K}$-$\bar{M}$ and $\bar{\Gamma}$-$\bar{M}$-$\bar{\Gamma}$ directions. On the other hand, the surface state S_3 appears very strong at small emission angles in both directions. In the $\bar{\Gamma}$-$\bar{K}$-$\bar{M}$ direction S_3 is only resolved between 0° and 20° while in the $\bar{\Gamma}$-$\bar{M}$-$\bar{\Gamma}$ directions it is well resolved at every emission angle. The surface state S_4 is only observed in the $\bar{\Gamma}$-$\bar{K}$-$\bar{M}$ direction and is first shown up at an emission angle of 12°. At 26° S_4 reaches its maximum and then it becomes weaker with higher emission angles. The fifth surface state S_5 is clearly resolved at an emission angle of 12° in the $\bar{\Gamma}$-$\bar{K}$-$\bar{M}$ and at 8° in the $\bar{\Gamma}$-$\bar{M}$-$\bar{\Gamma}$.

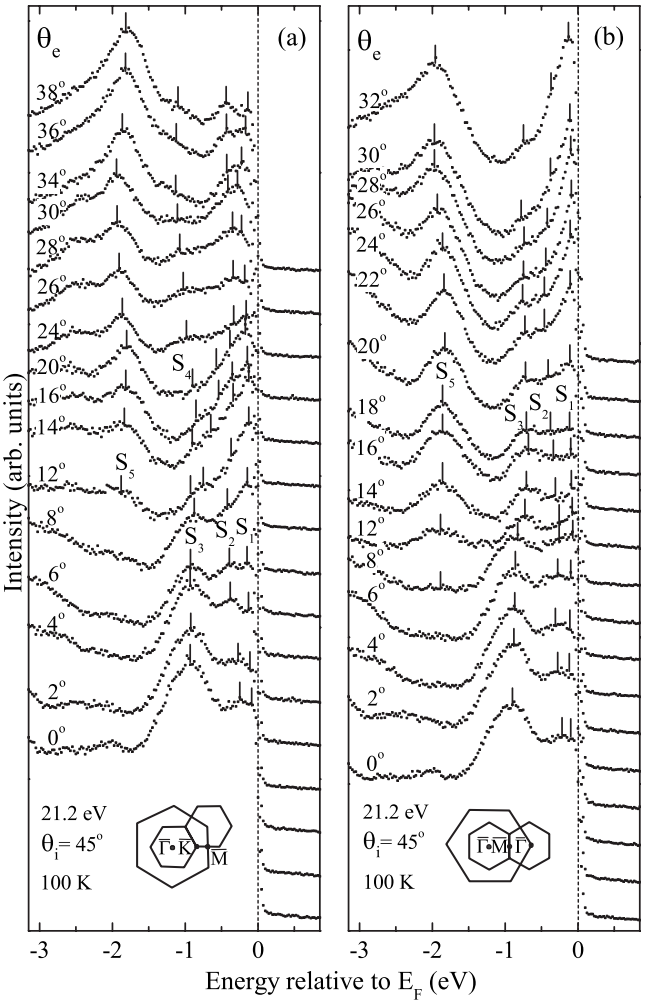

FIG. 2. ARPES spectra with various emission angles recorded at 100 K along the (a) $\bar{\Gamma}$-$\bar{K}$-$\bar{M}$ and (b) $\bar{\Gamma}$-$\bar{M}$-$\bar{\Gamma}$ lines of the surface $\sqrt{3}\times\sqrt{3}$ SBZ. The photon energy was 21.2 eV and the incidence angle for the photons was 45°. The five surface states are clearly observed and labeled as S_1–S_5.

At high emission angles this surface state becomes a distinct peak in both directions.

The k-resolved energy dispersion $E(k)$ of these states are displayed in Fig. 3, where the main part is obtained from the spectra in Figs. 2(a) and 2(b). The shaded area represents the Si bulk bands projected onto the 1×1 SBZ. At the $\bar{\Gamma}$ point S_1 is located 0.13 eV below the Fermi level and has a bandwidth of 0.2 eV. This state forms a continuous band as it is resolved at every $k_{\|}$ point in both the $\bar{\Gamma}$-$\bar{K}$-$\bar{M}$ and the $\bar{\Gamma}$-$\bar{M}$-$\bar{\Gamma}$ directions. The surface state S_2 is located 0.28 eV below the Fermi level at the $\bar{\Gamma}$ point and has a bandwidth of 0.25 eV. In the $\bar{\Gamma}$-$\bar{K}$-$\bar{M}$ direction it follows the periodicity of the $\sqrt{3}\times\sqrt{3}$ SBZ since it has a local maximum at the $\bar{M}$ point, and local minima close to the first and second $\bar{K}$ points. In the $\bar{\Gamma}$-$\bar{M}$-$\bar{\Gamma}$ direction it has a local maximum at the second $\bar{\Gamma}$ point, and a local minimum between the $\bar{M}$ point and the second $\bar{\Gamma}$ point. S_3 is located 0.98 eV below the Fermi level at the $\bar{\Gamma}$ point and has a bandwidth of 0.3 eV. In the $\bar{\Gamma}$-$\bar{K}$-$\bar{M}$

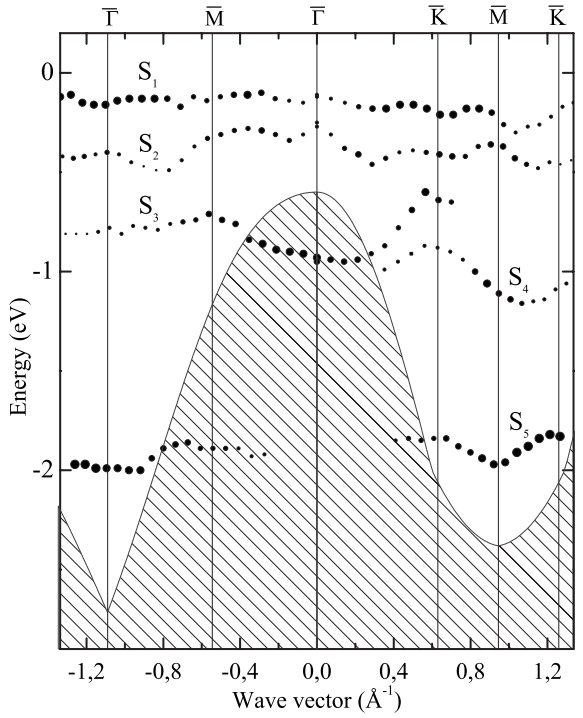

FIG. 3. Band mapping scheme showing the dispersion of the surface states along the $\bar{\Gamma}$-$\bar{M}$-$\bar{\Gamma}$ and the $\bar{\Gamma}$-$\bar{K}$-$\bar{M}$ directions of the $\sqrt{3}\times\sqrt{3}$ surface Brillouin zone. Parts of the original spectra are shown in Fig. 2. The spot size represents the intensity of the states at different emission angles. The surface states are labeled as S_1–S_5. The shaded area represents the projection of the Si bulk bands on the 1×1 SBZ.

direction it has a maximum close to the first $\bar{K}$ point while in the $\bar{\Gamma}$-$\bar{M}$-$\bar{\Gamma}$-direction it has a local maximum at the $\bar{M}$ point, and thus appears to follow the $\sqrt{3}$ periodicity. The surface state S_4 is only resolved in the $\bar{\Gamma}$-$\bar{K}$-$\bar{M}$ direction. It has a local maximum at the first $\bar{K}$ point and a local minimum close to the $\bar{M}$ point. The surface state S_4 is most likely not related to S_3 since they are located at different binding energies at the two $\bar{M}$ points. In the $\bar{\Gamma}$-$\bar{K}$-$\bar{M}$ direction the surface state S_5 has two local maxima close to the first and second $\bar{K}$ points, and one minimum at the $\bar{M}$ point. Evidently S_5 follows the periodicity of the $\sqrt{3}\times\sqrt{3}$ surface Brillouin zone. In the $\bar{\Gamma}$-$\bar{M}$-$\bar{\Gamma}$ direction it has a small dispersion and no distinct maximum or minimum is observed. The bandwidth of S_5 is around 0.2 eV.

In earlier valence-band PES studies, two main peaks were observed.[9–11] One sharp peak located ~0.15 eV below the Fermi level was assigned to Mn 3*d* states and a second broad peak located ~1.7 eV below the Fermi level was assigned to the Mn 3*d*-Si 3*sp* derived bonding states. Comparing our angle-resolved photoelectron spectroscopy (ARPES) spectra with the previous data, one finds that the peak close to the Fermi level in Refs. 9 and 10 consists of four surface states. That is, one intense peak (S_1) close to the Fermi level and three more states with higher binding energies (S_2, S_3, and S_4). The three latter states are not as intense as S_1 and could appear as a tail to the main peak close to the Fermi level in an integrated PES spectrum. The second broad peak in Refs. 9 and 10 is similar to the surface state S_5 as they are located at similar energy below the Fermi level.

Figure 4 shows high-resolution Si 2*p* core-level spectra. In order to fit the spectra over the entire energy and angular range, a combined Shirley and parabolic background has been used.[17] In the fitting program,[18] Voigt line shapes were used with a Doniach-Šunjić singularity index of $\alpha=0.04$ for all spectra in order to take care of the metallic tails.[19] The Lorentzians were held constant at 0.085 eV and the spin-orbit split at 0.602 eV. The branching ratios were varied between 0.45–0.55 for all components. The details about the line fit are listed in Table I. Figure 4(a) shows the bulk sensitive spectrum recorded at a photon energy of 108 eV. Two components and a parabolic background are used to get a satisfactory fitting. The main component is identified as a contribution from the silicon bulk. Since at this photon energy the mean-free path of the electrons is large, one expects to have a dominant contribution from the bulk. The second component, labeled as C_2, is shifted toward lower binding energy by -0.266 ± 0.025 eV. The details about this component are going to be discussed below.

For the spectra in Figs. 4(b)–4(h), recorded at photon energies from 120 to 140 eV, three more components, in addition to the bulk and C_2 components, are needed to fit the spectra in a satisfactory way. The existence of four components: B, C_1, C_2, and C_3, are clearly visible as peaks or shoulders in the raw spectra in Figs. 4(b)–4(h). These four components proved insufficient to achieve a good fit and the fifth component C_4 had to be introduced to obtain a consistent fit for all spectra over the whole energy and angular range. Compared to the bulk component B, C_1 is shifted toward lower binding energy by -0.723 ± 0.025 eV, and C_3 and C_4 are shifted to higher binding energy by 0.184 ± 0.011 and 0.458 ± 0.010 eV, respectively.

The Si 2*p* spectra, recorded with photon energies 130, 135, and 140 eV in Figs. 4(c)–4(e), are more surface sensitive than the spectra in Figs. 4(a) and 4(b) since with higher photon energy the mean-free path of the electrons decreases and reaches its minimum at a photon energy around 135–140 eV.[20,21] It can be seen in Figs. 4(a)–4(e) that the C_1 component increases in intensity with higher photon energy. This implies that C_1 is surface related. Also, in the most surface sensitive spectra recorded at 60° emission angles [Figs. 4(f)–4(h)], this component becomes stronger compared to the normal-emission spectra. These facts, together with the relative intensities in Table I, indicate that C_1 is a surface component.

C_2, which is already present in the 108 eV spectrum, has an increased intensity in the spectrum recorded at a photon energy of 120 eV [Fig. 4(b)]. In the more surface sensitive spectra recorded at 130–140 eV [Figs. 4(c)–4(e)], C_2 decreases slightly in intensity. This behavior implies a more bulklike character for C_2.

As expected, the bulk component B is continuously dropping in intensity from about 75% in the 108 eV spectrum to about 25% in the 140 eV spectrum [Figs. 4(a)–4(d)]. Comparing the normal-emission spectrum recorded at 120 eV [Fig. 4(b)] with the more surface sensitive spectrum [Fig.

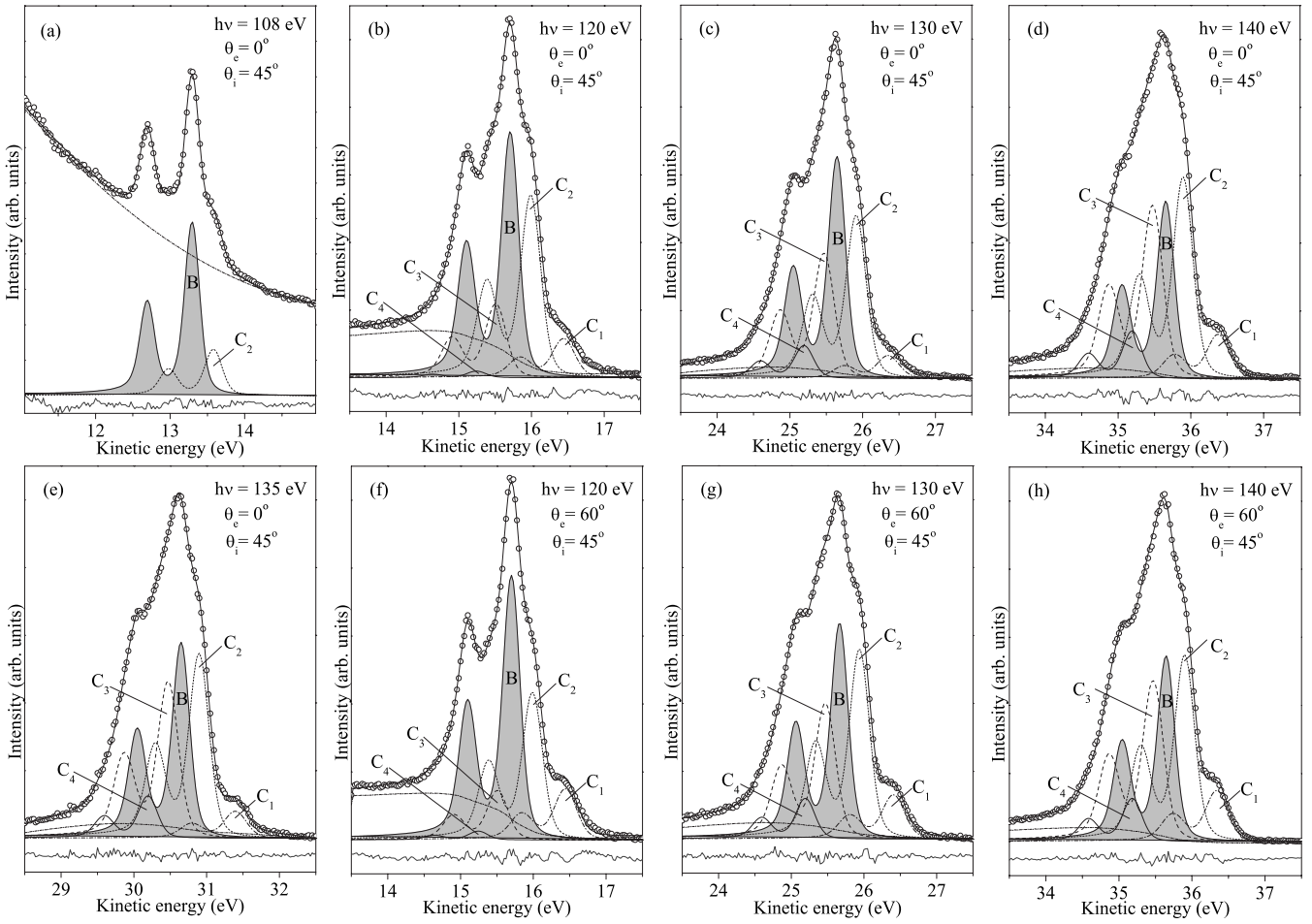

FIG. 4. High-resolution Si 2*p* core-level spectra recorded at 100 K, [(a)–(e)] normal emission, and [(f)–(h)] 60° emission. All the incident angles were 45°. The spectra were recorded with a photon energy of (a) 108, [(b) and (f)] 120, [(c) and (g)] 130, and [(d) and (h)] 140 eV. The solid lines show the total contribution from the components used to fit the experimental data (circles). Underneath each spectrum, the residual lines from the fitting procedure are presented.

4(f)] recorded at the same energy, the bulk component is increasing in intensity. This behavior is contrary to the bulk character seen by varying the photon energy, and is most likely caused by photoelectron diffraction effects.

The third surface component C_3, shifted toward higher binding energy, has a low intensity in the normal-emission spectrum recorded at 120 eV [Fig. 4(b)]. But it is continuously increasing in intensity in the successively more surface sensitive spectra [Figs. 4(c)–4(e)]. In the high emission angle spectra [Figs. 4(f)–4(h)], the intensity of C_3 is increasing in a similar way. The intensity of the fourth surface component C_4 behaves the same way as C_3.

TABLE I. Parameter details used to fit the spectra in Figs. 4(b)–4(h). In all spectra the Lorentzian FWHMs were kept constant at 0.085 eV and the spin-orbit splitting at 0.602 eV. The branching ratios were allowed to vary between 0.45 and 0.55. A singularity index of $\alpha = 0.04$ has been used in all the spectra. Peak intensity variations are shown in percent (%) of the total intensity.

			Intensity (%)							
	Binding energy shift	Gaussian FWHM	108 eV	120 eV		130 eV		135 eV	140 eV	
Component	(eV)	(eV)	0°	0°	60°	0°	60°	0°	0°	60°
Bulk (B)		0.225	75.9	41.3	46.6	35.3	32.1	29.4	24.5	26.6
C_1	−0.723 ± 0.025	0.310		8.2	11.5	4.8	8.2	5.2	8.0	9.4
C_2	−0.266 ± 0.025	0.269	24.1	34.6	30.0	29.9	30.9	30.9	31.6	30.0
C_3	0.184 ± 0.011	0.280		14.6	10.2	24.1	23.2	27.6	28.6	27.2
C_4	0.458 ± 0.010	0.257		1.2	1.7	5.9	6.5	6.9	7.3	6.8

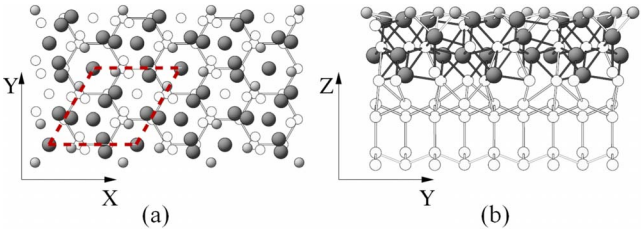

FIG. 5. (Color online) Atomic structure model of the MnSi film with B20 structure, from Ref. 22. (a) Top view with the $\sqrt{3}\times\sqrt{3}$ unit cell indicated by the dashed line. (b) Side view of the film structure in (a). Small spheres represent Si atoms with top-layer atoms shaded and large dark spheres are Mn atoms. The hexagonal bonding pattern in (a) displays the Si substrate lattice.

In order to explain the line profiles, we have compared our results to recent density-functional theory (DFT) calculations, in which a layered silicide structure has been suggested.[22] In this model the MnSi film can be matched to the Si(111) substrate due to the similar size of the Si(111)-$\sqrt{3}\times\sqrt{3}$ and the MnSi(111)-1×1 unit cells. The film is built up of alternating layers of manganese and silicon. The so-called dense and sparse atomic layers contain three and one atom per (1×1) unit cell of MnSi(111), respectively. The film is built up of two dense and two sparse Mn layers. First, the interface is formed by a dense layer of Si atoms followed by a sparse Mn layer, a sparse Si layer, and a dense Mn layer. Second, this stacking sequence is done twice. Finally, the film is terminated by a dense Si layer. In total, the amount of Mn in this model is close to three ML and each bulk unit cell of the MnSi contains eight Mn and eight Si atoms. In Figs. 5(a) and 5(b) the atomic structure of this film is shown in top and side views.

From the line-shape analysis one finds that the intensity of C_3 is three or four times larger than that of C_1 and C_3 is the most surface sensitive component (see Table I). These facts strongly suggest that C_3 may originate from the dense silicon layer that terminates the surface and forms the well-ordered $\sqrt{3}\times\sqrt{3}$ surface. According to the model of Ref. 22, C_1 should have its origin from the first sparse silicon layer. This is consistent with the size of C_1 compared to C_3. It is interesting to note that C_1 has a similar energy shift as the rest atoms of the clean Si(111)-7×7 surface, although, in the Si(111)-7×7 case, the shift to lower binding energy is caused by charge transfer from the adatoms to the dangling bonds of the rest atoms.[20] Also, since C_1 is clearly resolved already at a photon energy of 120 eV, the origin for this component might be from a layer beneath the topmost one. In Table I the Gaussian width of C_1 appears larger than the others. This can be explained by the extra atoms on top of the $\sqrt{3}$ surface, which has been observed by STM.[11] These extra atoms cause a disorder at the present site and result in a broader Gaussian width.

The intensity of C_2 varies only little among all the spectra and indicates that C_2 originates from layers below the surface. Also, the appearance of C_2 in the bulk sensitive 108 eV spectrum clearly indicates a component that originates from layers deep in the film, e.g., the Mn silicide. It is clear that component B is the contribution from the Si bulk because of its high intensity in the 108 eV spectrum [Fig. 4(a)] and its low intensity in the more surface sensitive spectra. The last component C_4 cannot be particularly associated with a specific silicon site in the current model. There are, however, two possible origins for this component, i.e., it is related to disorder in the film or on the surface.

In earlier photoemission studies, Kumar *et al.*[11] used three components to fit a spectrum from a similar $\sqrt{3}$ surface. Two components shifted toward lower binding energies with respect to the bulk component by −0.23 and −0.58 eV. The first component was identified as a contribution from the silicide, which is in agreement with our results concerning the similar core-level shift of C_2. We do not find a clear similarity to the second component in Ref. 11. But it is most likely related to C_1 in our paper since these two components have a similar behavior in both experiments. On the other hand, Magnano *et al.*[9] only used two components to fit a Si $2p$ spectrum for a similar surface. In that study the bulk component was completely suppressed for the MnSi film. They found that two components were shifted by −0.182 and −0.53 eV compared to the bulk component recorded for the clean Si(111)-7×7 surface. Obviously, the previous fitting of the Si $2p$ with three broad components is in contrast with our results. In our photoemission spectra, five components are needed to achieve a consistent fit over the whole energy and angle range. As evidenced by small peaks and shoulders in the raw spectra, the Si $2p$ core levels presented here are well resolved compared with those in Refs. 9 and 11. Besides differences at sample temperatures (the current experiment was done at 100 K while the earlier ones were at room temperature), there might be also Mn coverage differences among these experiments. We found that the Mn/Si(111)-$\sqrt{3}\times\sqrt{3}$ LEED pattern is insensitive to excess Mn coverage. Further deposition of Mn after 3 ML coverage only results in an island formation of Mn silicide with the $\sqrt{3}\times\sqrt{3}$ on the top. Consequently, it could strongly affect the Si $2p$ line shape.

IV. CONCLUSIONS

In conclusion, the surface electronic structure of Mn/Si(111)-$\sqrt{3}\times\sqrt{3}$ has been investigated by ARPES. Five surface states are found in the $\bar{\Gamma}$-$\bar{K}$-$\bar{M}$ direction and four in the $\bar{\Gamma}$-$\bar{M}$-$\bar{\Gamma}$ direction. In comparison with earlier results, a more detailed analysis of the surface contributions from the Si $2p$ spectra has been presented here. The reconstruction of the $\sqrt{3}\times\sqrt{3}$ surface has been discussed and compared to a theoretical model. Our photoemission data favor a Mn/Si(111)-$\sqrt{3}\times\sqrt{3}$ model that consists of the top $\sqrt{3}\times\sqrt{3}$ surface, the Mn silicide, and the bulk structure.

ACKNOWLEDGMENTS

The authors would like to thank the Swedish National Graduate School in Materials Science and the MAX-lab staff, as well as Peter Kratzer for letting us use the image of the atomic structure. This work was supported by the Swedish Research Council.

*Joakim.Hirvonen@kau.se

[1] S. A. Wolf, D. D. Awschalom, R. A. Buhrman, J. M. Daughton, S. von Molnar, M. L. Roukes, A. Y. Chtchelkanova, and D. M. Treger, Science **294**, 1488 (2001).
[2] T. Nagao, S. Ohuchi, Y. Matsuoka, and S. Hasegawa, Surf. Sci. **419**, 134 (1999).
[3] S. M. Shivaprasad, C. Anandan, S. G. Azatyan, Y. L. Gavriljuk, and V. G. Lifshits, Surf. Sci. **382**, 258 (1997).
[4] M. M. R. Evans, J. C. Glueckstein, and J. Nogami, Phys. Rev. B **53**, 4000 (1996).
[5] K. Schwinge, J. J. Paggel, and P. Fumagalli, Surf. Sci. **601**, 810 (2007).
[6] G. Ctistis, U. Deffke, J. J. Paggel, and P. Fumagalli, J. Magn. Magn. Mater. **240**, 420 (2002).
[7] G. Ctistis, U. Deffke, K. Schwinge, J. J. Paggel, and P. Fumagalli, Phys. Rev. B **71**, 035431 (2005).
[8] K. H. Kim, S. W. Han, J. D. Lee, J. J. Lee, K. J. Kim, B. S. Kim, S. C. Wi, S. S. Lee, G. Kim, and J.-S. Kang, J. Korean Phys. Soc. **48**, 5 (2006).
[9] E. Magnano, E. Carleschi, A. Nicolaou, T. Pardini, M. Zangrando, and F. Parmigiani, Surf. Sci. **600**, 3932 (2006).
[10] E. Carleschi, E. Magnano, M. Zangrando, F. Bondino, A. Nicolaou, F. Carbone, D. Van der Marel, and F. Parmigiani, Surf. Sci. **601**, 4066 (2007).
[11] A. Kumar, M. Tallarida, M. Hansmann, U. Starke, and K. Horn, J. Phys. D **37**, 1083 (2004).
[12] S. Kawamoto, M. Kusaka, M. Hirai, and M. Iwami, Surf. Sci. **242**, 331 (1991).
[13] K. Adambaev, A. Yusupov, and K. Yakubov, Inorg. Mater. **39**, 942 (2003).
[14] B. N. Jensen, S. M. Butorin, T. Kaurila, R. Nyholm, and L. I. Johansson, Nucl. Instrum. Methods Phys. Res. A **394**, 243 (1997).
[15] J. Hirvonen Grytzelius, H. M. Zhang, and L. S. O. Johansson (unpublished).
[16] R. Losio, K. N. Altmann, and F. J. Himpsel, Phys. Rev. B **61**, 10845 (2000).
[17] D. A. Shirley, Phys. Rev. B **5**, 4709 (1972).
[18] D. L. Adams and J. N. Andersen, FITXPS Version 2.12, freely downloadable from http://www.sljus.lu.se/download.html, 2006.
[19] S. Doniach and M. Šunjić, J. Phys. C **3**, 285 (1970).
[20] C. J. Karlsson, E. Landemark, Y.-C. Chao, and R. I. G. Uhrberg, Phys. Rev. B **50**, 5767 (1994).
[21] J. J. Paggel, W. Thesis, K. Horn, Ch. Jung, C. Hellwig, and H. Petersen, Phys. Rev. B **50**, 18686 (1994).
[22] M. Hortamani, P. Kratzer, and M. Scheffler, Phys. Rev. B **76**, 235426 (2007).